Chapter 17

Instabilities of Rotating Stratified Flows

ABSTRACT

In a stratified rotating fluid, not all geostrophic flows are stable, for some are vulnerable to growing perturbations. This chapter presents two primary mechanisms by which instability may occur: motion of individual particles (called *inertial instability*) and organized motions across the flow (called *baroclinic instability*). In each case, kinetic energy is supplied to the disturbance by release of potential energy from the original flow. Baroclinic instability is at the origin of the midlatitude cyclones and anticyclones that make our weather so variable. Because the evolution of weather perturbations is essentially nonlinear, a two-layer quasi-geostrophic model is presented here to simulate the evolution of the baroclinic instability past the linear-growth phase.

17.1 TWO TYPES OF INSTABILITY

There are two broad types of flow instability. One is *local* or *punctual* in the sense that every particle in (at least a portion of) the flow is in an unstable situation. A prime example of this type is gravitational instability, which occurs in the presence of a reverse stratification (top-heavy fluid): if displaced, either upward or downward, a particle is subjected to a buoyancy force that pulls it further away from its original location and, since all other particles are individually subjected to a similar pull, the result is a catastrophic overturn of the fluid followed by mixing. In the absence of friction, there is no specific temporal and spatial scales for the event.

The second type of instability can exist only if the flow is stable with respect to the first kind. It is more gradual and relies on a collaborative action of many, if not all, particles and for this reason can be called *global* or *organized*. The instability is manifested by the temporal growth of a wave at a preferential wavelength that eventually overturns and forms vortices. An example is the barotropic instability encountered in Chapter 10 (see Section 10.4 in particular).

Rotating stratified flows can be subjected to either type of instability. If the instability is local, it is called *inertial instability*, and if it is global, *baroclinic*

Introduction to Geophysical Fluid Dynamics, Volume 101, ISSN 0074-6142, DOI: 10.1016/B978-0-12-088759-0.00017-1

TABLE 17.1 Contrasting Characteristics of the Two Types of Instability to which a Fluid Flow May Be Subjected

Local Instability	Global Instability
Particles act individually.	Particles act in concert.
Motion proceeds randomly.	Motion proceeds in a wave arrangement.
Instability criterion depends only on local properties of the flow.	Instability criterion depends on bulk properties of the flow and on wavelength of perturbation.
Instability is independent of boundary conditions.	Instability is sensitive to boundary conditions.
Instability is catastrophic (major overturn, mixing).	Instability is gradual (growing wave and vortex formation).
Example: overturning of a top-heavy fluid	Example: Kelvin–Helmholtz instability
In rotating stratified flow: inertial instability	In rotating stratified flow: mixed barotropic–baroclinic instability

instability. Table 17.1 summarizes the contrasting properties of the two types of instabilities.

Baroclinic instability is actually an end member of a more general instability, called *mixed barotropic–baroclinic instability*, which occurs when the flow is sheared in both horizontal and vertical directions. Baroclinic instability is the extreme when there is no shear in the horizontal, and barotropic instability (Chapter 10) is the other extreme, when the original flow has a no shear in the vertical.

17.2 INERTIAL INSTABILITY

In this section, we consider the possibility of catastrophic instability, namely one in which a fluid particle once displaced from its position of equilibrium keeps moving further away from that position. Such instability is catastrophic because, if one such particle migrates away from its initial position, all others can do so as well, and the ensuing situation is overturn, mixing and chaos.

This instability can be characterized also as *inertial* because acceleration is the crux of the growing displacement of the particles in the system. Finally, inertial instability is sometimes called *symmetric instability* (Holton, 1992) due to some symmetry in its formulation, as the following developments will shortly reveal.

Let us consider an inviscid steady flow in thermal-wind balance with variation across the vertical plane (x, z), with sheared velocity $v(x, z)$ in equilibrium with a slanted stratification $\rho(x, z)$. Such flow must be both geostrophic and hydrostatic:

$$-fv = -\frac{1}{\rho_0}\frac{\partial p}{\partial x} \tag{17.1a}$$

$$0 = -\frac{1}{\rho_0}\frac{\partial p}{\partial z} - \frac{g\rho}{\rho_0}. \tag{17.1b}$$

Elimination of pressure p between these two equations yields the thermal-wind balance

$$f\frac{\partial v}{\partial z} = -\frac{g}{\rho_0}\frac{\partial \rho}{\partial x}. \tag{17.2}$$

From these flow characteristics, let us define the stratification frequency N by

$$N^2 = -\frac{g}{\rho_0}\frac{\partial \rho}{\partial z} = \frac{1}{\rho_0}\frac{\partial^2 p}{\partial z^2}, \tag{17.3}$$

and, similarly, two quantities that will be become useful momentarily:

$$F^2 = f\left(f + \frac{\partial v}{\partial x}\right) = f^2 + \frac{1}{\rho_0}\frac{\partial^2 p}{\partial x^2} \tag{17.4}$$

$$fM = f\frac{\partial v}{\partial z} = -\frac{g}{\rho_0}\frac{\partial \rho}{\partial x} = \frac{1}{\rho_0}\frac{\partial^2 p}{\partial x \partial z}. \tag{17.5}$$

Note that the three quantities N^2, F^2, and fM all have the dimension of a frequency squared. But, although the first two are defined as squares, we ought to entertain the possibility that they may be negative.

Next, let us perturb such flow by adding time dependency and velocity components u and w within the x–z plane, while assuming still no variation in the perpendicular direction. For clarity of exposition, we further assume inviscid flow and restrict the attention to the f-plane, but we allow for possible nonhydrostaticity in the vertical, in anticipation of large vertical accelerations:

$$\frac{\mathrm{d}u}{\mathrm{d}t} - fv = -\frac{1}{\rho_0}\frac{\partial p}{\partial x} \tag{17.6a}$$

$$\frac{\mathrm{d}v}{\mathrm{d}t} + fu = 0 \tag{17.6b}$$

$$\frac{\mathrm{d}w}{\mathrm{d}t} = -\frac{1}{\rho_0}\frac{\partial p}{\partial z} - \frac{g\rho}{\rho_0}, \tag{17.6c}$$

where $\mathrm{d}/\mathrm{d}t$ stands for the material derivative (following particle movement).

In this flow, let us track an individual fluid particle with moving coordinates $[x(t), z(t)]$. Its velocity components in the vertical plane are

$$u = \frac{\mathrm{d}x}{\mathrm{d}t}, \qquad w = \frac{\mathrm{d}z}{\mathrm{d}t}, \tag{17.7}$$

which transform Eq. (17.6b) into

$$\frac{\mathrm{d}v}{\mathrm{d}t} + f\,\frac{\mathrm{d}x}{\mathrm{d}t} = 0. \tag{17.8}$$

Since f is constant in our model, the quantity $v + fx$ is an invariant of the motion,[1] and it follows that if the particle is displaced horizontally over a distance Δx it undergoes a change of transverse velocity Δv such that

$$\Delta v + f\Delta x = 0. \tag{17.9}$$

Turning our attention to Eqs. (17.6a) and (17.6c) and eliminating from them u and w by using (17.7), we obtain

$$\frac{\mathrm{d}^2x}{\mathrm{d}t^2} - fv = -\frac{1}{\rho_0}\,\frac{\partial p}{\partial x} \tag{17.10a}$$

$$\frac{\mathrm{d}^2z}{\mathrm{d}t^2} = -\frac{1}{\rho_0}\,\frac{\partial p}{\partial z} - \frac{g\rho}{\rho_0}. \tag{17.10b}$$

Note that in these equations the pressure terms on the right-hand side are complicated functions of the particle position (x, z).

Let us now imagine that the fluid particle under consideration is only moved from its original position by a small displacement Δx in the horizontal and Δz in the vertical: $x(t) = x_0 + \Delta x(t)$, $z(t) = z_0 + \Delta z(t)$, so that we may linearize the equations. Note that any displacement along y has no effect on the dynamic balance and can be ignored. Neglecting compressibility effects, we assume that the displacement causes no change in density for the particle. At its new position, the particle is out of equilibrium. In the vertical, it is subject to a buoyancy force, while in the horizontal, it is no longer in geostrophic equilibrium. These forces are reflected in the new, local values of the pressure gradient, which for a small displacement can be obtained from the original values by a Taylor expansion:

$$\left.\frac{\partial p}{\partial x}\right|_{\text{at } x+\Delta x, z+\Delta z} = \left.\frac{\partial p}{\partial x}\right|_{\text{at } x,z} + \Delta x\left.\frac{\partial^2 p}{\partial x^2}\right|_{\text{at } x,z} + \Delta z\left.\frac{\partial^2 p}{\partial x \partial z}\right|_{\text{at } x,z} \tag{17.11a}$$

$$\left.\frac{\partial p}{\partial z}\right|_{\text{at } x+\Delta x, z+\Delta z} = \left.\frac{\partial p}{\partial z}\right|_{\text{at } x,z} + \Delta x\left.\frac{\partial^2 p}{\partial x \partial z}\right|_{\text{at } x,z} + \Delta z\left.\frac{\partial^2 p}{\partial z^2}\right|_{\text{at } x,z}. \tag{17.11b}$$

[1] This is occasionally called the *geostrophic momentum*.

After subtraction of the unperturbed state, the equations governing the evolution of the displacement are

$$\frac{\mathrm{d}^2\Delta x}{\mathrm{d}t^2} - f\Delta v = -\frac{1}{\rho_0}\left(\frac{\partial^2 p}{\partial x^2}\right)\Delta x - \frac{1}{\rho_0}\left(\frac{\partial^2 p}{\partial x \partial z}\right)\Delta z \tag{17.12a}$$

$$\frac{\mathrm{d}^2\Delta z}{\mathrm{d}t^2} = -\frac{1}{\rho_0}\left(\frac{\partial^2 p}{\partial x \partial z}\right)\Delta x - \frac{1}{\rho_0}\left(\frac{\partial^2 p}{\partial z^2}\right)\Delta z, \tag{17.12b}$$

in which $\Delta v = -f\Delta x$ according to (17.9). The first equation tells that the force imbalance in the x-direction is due in part to the Coriolis force having changed by $f\Delta v$ and in part to immersion in a new pressure gradient. By Newton's second law, this causes a horizontal acceleration $\mathrm{d}^2\Delta x/\mathrm{d}t^2$. Likewise, the second equation states that the modified pressure environment causes an imbalance in the vertical. The new neighbors together exert a buoyancy force on our particle, and the latter acquires a vertical acceleration $\mathrm{d}^2\Delta z/\mathrm{d}t^2$.

Since the equations are now linear, we may seek solutions of the form

$$\Delta x = X\exp(\mathrm{i}\omega t), \qquad \Delta z = Z\exp(\mathrm{i}\omega t). \tag{17.13}$$

If the frequency ω is real, the particle oscillates around its original position of equilibrium, and the flow can be characterized as stable. On the contrary, should ω be complex and have a negative imaginary part, the solution includes exponential growth, the particle drifts away from its original position, and the flow is deemed to be unstable.

Substitution on the solution type in the governing equations yields a two-by-two system for the amplitudes X and Z:

$$(F^2-\omega^2)\Delta x + fM\Delta z = 0 \tag{17.14a}$$

$$fM\Delta x + (N^2-\omega^2)\Delta z = 0, \tag{17.14b}$$

in which we introduced quantities defined in (17.3), (17.4), and (17.5). A nonzero solution exists only if ω obeys

$$(F^2-\omega^2)(N^2-\omega^2) = f^2M^2, \tag{17.15}$$

of which the ω^2 roots are

$$\omega^2 = \frac{F^2+N^2 \pm \sqrt{(F^2-N^2)^2+4f^2M^2}}{2}. \tag{17.16}$$

The question is whether one or both ω^2 values can be negative, in which case there is at least one ω root with a negative imaginary part.

Before proceeding with the general case, it is instructive to consider two extreme cases. First is the case of stratification without rotation (v is a constant and ρ is a function of z only; $F^2 = fM = 0$ and $N^2 \neq 0$), for which

$$\omega^2 = \frac{N^2 \pm \sqrt{N^4}}{2} = 0 \text{ or } N^2. \tag{17.17}$$

All ω values are real if $N^2 \geq 0$, which corresponds to a density increasing downward ($d\rho/dz < 0$). Otherwise the fluid is top heavy and overturns. This is gravitational instability first encountered in Section 11.2.

The second extreme case is that of a pure shear (v is a function of x only and ρ is a constant: $F^2 \neq 0$ and $fM = N^2 = 0$), for which

$$\omega^2 = \frac{F^2 \pm \sqrt{F^4}}{2} = 0 \text{ or } F^2. \tag{17.18}$$

All ω values are real if $F^2 \geq 0$, which corresponds to $f(f + \partial v/\partial x) \geq 0$, that is, $(f + \partial v/\partial x)$ of the same sign as f. Should F^2 be negative, the flow mixes horizontally. This is inertial instability in a pure form.

This result is less intuitive than the first and begs for a physical explanation. So let us follow the evolution of a particle displaced laterally (Fig. 17.1). During the displacement Δx, it conserves its geostrophic momentum and sees its velocity v change according to (17.9). As it arrives at a new place, the Coriolis force exerted on the particle no longer matches the pressure gradient force, for the following two reasons: the particle's own velocity has changed and the pressure gradient is different at the new place. Hence the particle is

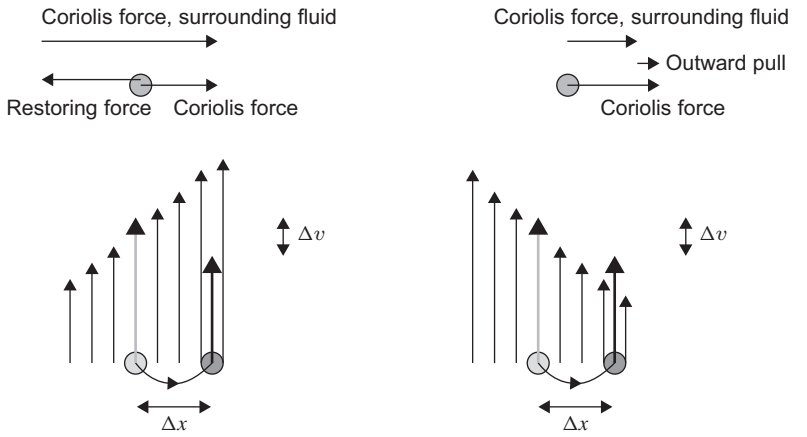

FIGURE 17.1 A fluid particle displaced to the right by a distance $\Delta x > 0$ conserves its geostrophic momentum and sees its velocity drop to $v(x) - f\Delta x$. In the case of the *left panel*, the new particle velocity is weaker than the ambient velocity $v(x + \Delta x) = v(x) + (dv/dx)\Delta x$ at its new place, and its own Coriolis force (from left to right) is insufficient to meet the local pressure-gradient force (from right to left). Consequently, the particle is subjected to a net residual force (from right to left) that pushes it back toward its original position, a restoring force. In the case of the *right panel*, the situation is reversed: the particle's new velocity exceeds the ambient velocity, and its Coriolis force (from left to right) is stronger than the local pressure-gradient force (from right to left), leaving a difference that pulls the particle from left to right and thus further away from its original place. The former case is stable, whereas the latter is unstable.

no longer in geostrophic equilibrium and undergoes a net acceleration in the x-direction. It is either pushed back toward its original location or further accelerated away from there, depending on how the particle's Coriolis force compares to the local pressure-gradient force. As shown in Fig. 17.1, in the northern hemisphere ($f > 0$), stability requires that a particle displaced to the right ($\Delta x > 0$) sees its new velocity $v - f\Delta x$ fall below the surrounding velocity $v + \Delta x(\partial v/\partial x)$ to be pushed back toward its original location, hence stability condition $f + \partial v/\partial x > 0$.

Returning to the general case, we realize that the switch between stability and instability occurs when $\omega^2 = 0$, which according to (17.16) occurs when

$$F^2N^2 = f^2M^2. \tag{17.19}$$

Around this relation, the signs of the ω^2 roots are as depicted in Fig. 17.2. It is clear from this graph that stability demands three conditions[2]:

$$F^2 \geq 0, \quad N^2 \geq 0, \quad \text{and} \quad F^2N^2 \geq f^2M^2. \tag{17.20}$$

The third condition is the most intriguing of the group and deserves some physical interpretation. For this, let us take F^2 and N^2 both positive and define the slope (positive downward) of the lines in the vertical (x, z) plane along which

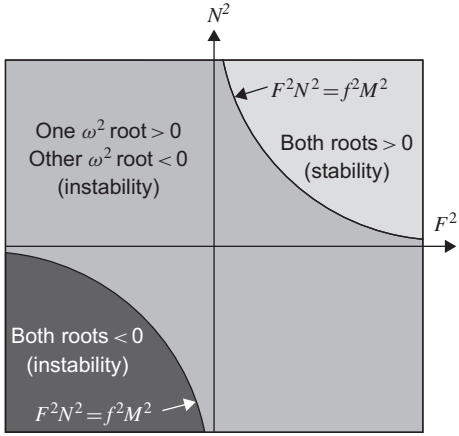

FIGURE 17.2 Stability diagram in the parameter space (F^2, N^2) for the inertial instability of a thermal-wind flow.

[2]Note that $F^2N^2 \geq f^2M^2$ alone is not sufficient because it could be obtained with F^2 and N^2 each negative.

the geostrophic momentum $v+fx$ and density ρ are constant:

$$\begin{aligned} S_{\text{momentum}} &= \text{slope of line } v+fx = \text{constant} \\ &= \frac{\partial(v+fx)/\partial x}{\partial(v+fx)/\partial z} = \frac{F^2}{fM} \end{aligned} \tag{17.21}$$

$$\begin{aligned} S_{\text{density}} &= \text{slope of line } \rho = \text{constant} \\ &= \frac{\partial\rho/\partial x}{\partial\rho/\partial z} = \frac{fM}{N^2}. \end{aligned} \tag{17.22}$$

The stability threshold $F^2N^2 = f^2M^2$ then corresponds to equal momentum and density slopes. Normally, the velocity varies strongly in x and weakly in z, whereas density behaves in the opposite way, varying more rapidly in z than in x. Typically, therefore, lines of equal geostrophic momentum are steeper than lines of equal density. It turns out that this is the stable case $F^2N^2 > f^2M^2$ (left panel of Fig. 17.3).

With increasing thermal wind, momentum lines become less inclined and density lines more steep, until they cross. Beyond this crossing, the steeper lines are the density lines, $F^2N^2 < f^2M^2$, and the system is unstable (right panel of Fig. 17.3). Particles quickly drift away from their initial position, and the fluid is vigorously rearranged until it becomes marginally stable, just as a top-heavy fluid ($N^2 < 0$) is gravitationally unstable and becomes mixed until its density is homogenized ($N^2 = 0$). In other words, a situation with density lines steeper than geostrophic lines cannot persist and rearranges itself quickly until these lines coincide.

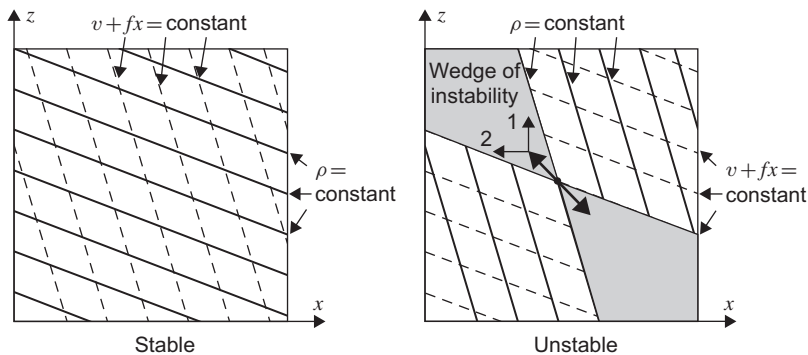

FIGURE 17.3 Left panel: Stability when lines of constant geostrophic momentum $v+fx$ are steeper than lines of constant density ρ. Right panel: Instability when lines of constant geostrophic momentum are less steep than lines of constant density; any particle (such as the one highlighted on the figure) displaced within the wedge is pulled further away by a combination of buoyancy force (1) and geostrophic imbalance (2).

In the unstable regime, it can be shown (see Analytical Problem 17.6) that growing particle displacements lie in the wedge between the momentum and density lines (right panel of Fig. 17.3). This justifies yet another name for the process: *wedge instability*.

17.3 BAROCLINIC INSTABILITY—THE MECHANISM

In thermal-wind balance, geostrophy and hydrostaticity combine to maintain a flow in equilibrium. Assuming that this flow is stable with respect to inertial instability (previous section), the equilibrium is not that of least energy, because a reduction in slope of density surfaces by spreading of the lighter fluid above the heavier fluid would lower the center of gravity and thus the potential energy. Simultaneously, it would also reduce the pressure gradient, its associated geostrophic flow and the kinetic energy of the system. Evidently, the state of rest is that of least energy (minimum potential energy and zero kinetic energy).

In a thermal wind, relaxation of the density distribution and tendency toward the state of rest cannot occur in any direct, spontaneous manner. Such an evolution would require vertical stretching and squeezing of fluid columns, neither of which can occur without alteration of potential vorticity.

Friction is capable of modifying potential vorticity, and under the slow action of friction a state of thermal wind decays, eventually bringing the system to rest. But there is a more rapid process that operates before the influence of friction becomes noticeable.

Vertical stretching and squeezing of fluid parcels is possible under conservation of potential vorticity if relative vorticity comes into play. As we have seen in Section 12.3, a column of stratified fluid that is stretched vertically develops cyclonic relative vorticity, and one that is squeezed acquires anticyclonic vorticity. In a slightly perturbed thermal-wind system, the vertical stretching and squeezing occurring simultaneously at different places generates a pattern of interacting vortices. Under certain conditions, these interactions can increase the initial perturbation, thus forcing the system to evolve away from its original state.

Physically, a partial relaxation of the density surfaces liberates some potential energy, while the concomitant stretching and squeezing creates new relative vorticity. The kinetic energy of the new motions can naturally be provided by the potential energy release. If conditions are favorable, these motions can then contribute to further relaxation of the density field and to stronger vortices. With time, large vortices can be formed at the expense of the original thermal wind. Vortices noticeably increase the amount of velocity shear in the system, greatly enhancing the action of friction. The evolution toward a lower energy level is therefore more effective via the transformation from potential energy into kinetic energy and generation of vortices than by friction acting on the thermal-wind flow.

Let us now investigate how a disturbance of a thermal-wind flow can generate a relative-vorticity distribution favorable to growth. For this purpose, a two-fluid idealization, as depicted in Fig. 17.4, is sufficient. For the discussion, let us also ignore the beta effect and align the x-direction with that of the thermal wind $(U_1 - U_2)$. The interface then slopes upward in the y-direction (middle

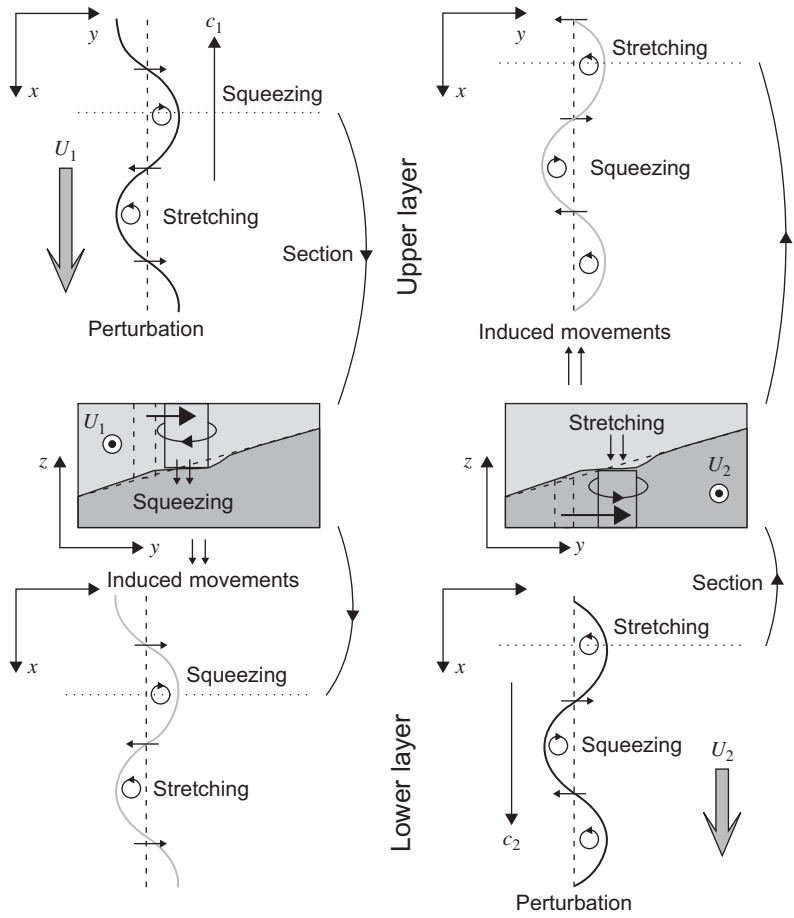

FIGURE 17.4 Patterns of squeezing and stretching caused by lateral displacements in a two-layer flow in thermal-wind balance. Squeezing generates anticyclonic vorticity (clockwise motion in the northern hemisphere), while stretching generates cyclonic vorticity (counterclockwise motion in the northern hemisphere). The flexibility of the density interface distributes the squeezing and stretching across both layers, and the result is that a cross-flow displacement in the upper layer (upper left of the figure) causes an accompanying pattern of squeezing and stretching in the lower layer (lower left of the figure). Vice versa, a cross-flow displacement in the lower layer (lower right of the figure) causes a similar pattern of squeezing and stretching in the upper layer (upper right of the figure). Growth occurs when the two sets of patterns mutually reinforce each other.

panels of Fig. 17.4). A perturbation of the upper flow causes some of its parcels to move in the $+y$-direction, into a shallower region (middle-left panel of the figure), and these undergo some vertical squeezing and thus acquire anticyclonic vorticity (clockwise in the figure). Because the density interface is not a rigid bottom but a flexible surface, it deflects slightly, relieving the upper parcels from some squeezing and creating a complementary squeeze in the lower layer. Thus, lower layer parcels, too, develop anticyclonic vorticity at the same location. Note that a lowering of the interface on the shallower side is also in the direction of a decrease of available potential energy.

Elsewhere, the disturbance causes upper layer parcels to move in the opposite direction—that is, toward a deeper region. There, vertical stretching takes place, and, again, because the interface is flexible, this stretching in the upper layer is only partial, the interface rises somewhat, and a complementary stretching occurs in the lower layer. Thus, parcels in both layers develop cyclonic relative vorticity (counterclockwise in the figure). Note that a lifting of the interface on the deeper side is again in the direction of a decrease of available potential energy. If the disturbance has some periodicity, as shown in the figure, alternating positive and negative displacements in the upper layer cause alternating columns of anticyclonic and cyclonic vorticities extending through both layers. Parcels lying between these columns of vortical motion are entrained in the directions marked by the arrows in the figure (upper left and lower left panels), creating subsequent displacements. Because these latter displacements occur not at but between the crests and troughs of the original displacements, they lead not to growth but to a translation of the disturbance.[3] Thus, a pattern of displacement in the upper layer generates a propagating wave. The direction of propagation (c_1 in upper left panel of Fig. 17.4) is opposite to that of the thermal wind ($U_1 - U_2$).

Similarly, cross-flow displacements in the lower layer (right panel of Fig. 17.4) generate patterns of stretching and squeezing in both layers. The difference is that, because of the sloping nature of the density interface, displacements in the $+y$-direction (middle-right panel in the figure) are accompanied by stretching instead of squeezing. Fluid parcels lying between vortical motions take their turn in being displaced, and the pattern again propagates as a wave (c_2 in lower right panel of Fig. 17.4), this time in the direction of the thermal wind.

By itself, each displacement pattern in a layer only generates a vorticity wave, but growth or decay of the whole can take place depending on whether the two separately induced patterns reinforce or negate each other. If the vorticity patterns induced by the upper layer and lower layer displacements are in quadrature with each other, the complementary vortical motions (upper right and upper left sides of Fig. 17.4, respectively) of one set fall at the crests and

[3]The mechanism here is identical to that of planetary and topographic waves, discussed in Section 9.6.

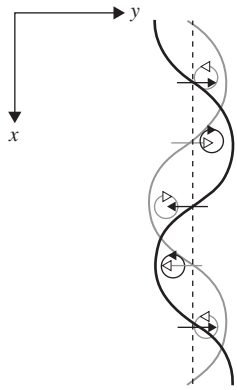

FIGURE 17.5 Interaction of displacement patterns and vortex tubes in the upper layer of a two-layer thermal-wind flow when displacements occur in both layers. The illustration depicts the case of a mutually reinforcing pair of patterns, when the vortical motions of one pattern act to increase the displacements of the other. A similar figure could be drawn for the lower layer, and it can be shown that, if the combination of patterns is self-reinforcing in one layer, it is self-reinforcing in the other layer, too. This is the essence of baroclinic instability.

troughs of the other set, and the ensuing interaction is either favorable or unfavorable to growth. If the spatial phase difference is such that the displacement pattern in one layer is shifted in the direction of the thermal-wind flow in that layer ($U_1 - U_2$ in the upper layer—the opposite in the lower layer), as depicted in Fig. 17.5, the vortical motions of one pattern act to increase the displacements of the other, and the disturbance in each layer amplifies that in the other. The system evolves away from its initial equilibrium.

The preceding description points to the need of a specific phase arrangement between the displacements in the two layers and emphasizes the role of vorticity generation. A further requirement is necessary for growth: the disturbance must have a wavelength that is neither too short nor too long and must be such that the vertical stretching and squeezing effectively generates relative vorticity. To show this in the simplest terms, let us consider the quasi-geostrophic form of the potential vorticity (16.17), on the f-plane:

$$q = \nabla^2\psi + \frac{\partial}{\partial z}\left(\frac{f^2}{N^2}\frac{\partial \psi}{\partial z}\right), \tag{17.23}$$

where ψ is the streamfunction, f the Coriolis parameter, N the stratification frequency, and ∇^2 the two-dimensional Laplacian. For a displacement pattern of wavelength L, the first term representing relative vorticity is on the the order of

$$\nabla^2\psi \sim \frac{\Psi}{L^2}, \tag{17.24}$$

where the streamfunction scale Ψ is proportional to the amplitude of the displacements. If the height of the system is H, the second term (representing vertical stretching) scales as

$$\frac{\partial}{\partial z}\left(\frac{f^2}{N^2}\frac{\partial \psi}{\partial z}\right) \sim \frac{f^2\Psi}{N^2H^2} = \frac{\Psi}{R^2}, \tag{17.25}$$

where we have defined the deformation radius $R = NH/f$.

Now, if L is much larger than R, the relative vorticity cannot match the vertical stretching as scaled. This implies that vertical stretching will be inhibited, and the displacements in the layers will tend to be in phase in order to reduce squeezing and stretching of fluid parcels in each layer. On the other hand, if L is much shorter than R, relative vorticity dominates potential vorticity. The two layers become uncoupled, and there is insufficient potential energy to feed a growing disturbance. In sum, displacement wavelengths on the order of the deformation radius are the most favorable to growth.

Another requirement for the two layers to interact is related to their relative propagation speed. It is clear that the interaction described above must be persistent in order to allow the positive feedback mechanism to continue. With propagating patterns in each layer this is only possible if the two features are moving at the same speed with respect to a fixed observer. The upper layer perturbation moves with a retrograde speed c_1 with respect to the flow velocity U_1, thus at speed $U_1 - c_1$. The lower layer perturbation moves at a forward speed c_2 with respect to the flow velocity U_2, thus at speed $U_2 + c_2$. For the layers to interact in a persistent matter, we therefore expect

$$U_1 - c_1 = U_2 + c_2. \tag{17.26}$$

Neglecting momentarily the asymmetry in wave propagation due to the beta effect, c_1 and c_2 are wave speeds of topographic waves associated with the sloping interface between the layers. For identical layer thicknesses, symmetry dictates $c_1 = c_2$, and condition (17.26) gives $c_1 = c_2 = (U_1 - U_2)/2$. The absolute propagation speed of the instability is $U_1 - c_1 = U_2 + c_2 = (U_1 + U_2)/2$, the average flow speed.

Because fluctuations are so ubiquitous in nature, an existing flow in thermal-wind balance will continuously be subjected to perturbations. Most of these will have a benign effect because they do not have the proper phase arrangement or a suitable wavelength. But, sooner or later, a perturbation with both favorable phase and wavelength will occur, prompting the system to evolve irreversibly from its equilibrium state. We conclude that flows in thermal-wind balance are intrinsically unstable. Because their instability process depends crucially on a phase shift with height, the fatal wave must have a baroclinic structure. To reflect this fact, the process is termed *baroclinic instability*.

The cyclones and anticyclones of our midlatitude weather are manifestations of the baroclinic instability of the atmospheric jet stream. The person who first analyzed the stability of vertically sheared currents (thermal wind) and who demonstrated the relevance of the instability mechanism to our weather is J. G. Charney.[4] While Charney (1947) performed the stability analysis for a continuously stratified fluid on the beta plane, Eady (1949) did the analysis on the f-plane independently. The comparison between the two theories reveals that

[4]For a short biography, see the end of Chapter 16.

the beta effect is a stabilizing influence. Briefly, a change in planetary vorticity (by meridional displacements) is another way to allow vertical stretching and squeezing while preserving potential vorticity. Relative vorticity is then no longer as essential and, in some cases, sufficiently suppressed to render the thermal wind stable to perturbations of all wavelengths.

17.4 LINEAR THEORY OF BAROCLINIC INSTABILITY

Numerous stability analyses have been published since those of Charney and Eady, exemplifying one aspect or another. Phillips (1954) idealized the continuous vertical stratification to a two-layer system, a case which Pedlosky (1963, 1964) generalized by allowing arbitrary horizontal shear in the basic flow, and Pedlosky and Thomson (2003) generalized to temporally oscillating basic flow. Barcilon (1964) studied the influence of friction on baroclinic instability by including the effect of Ekman layers, whereas Orlanski (1968, 1969) investigated the importance of non-quasi-geostrophic effects and of a bottom slope. Later, Orlanski and Cox (1973), Gill, Green and Simmons (1974), and Robinson and McWilliams (1974) confirmed that baroclinic instability is the primary cause of the observed oceanic variability at intermediate scales (tens to hundreds of kilometers).

Here, we only present one of the simplest mathematical models, taken from Phillips (1954), because it best exemplifies the mechanism described in the previous section. The fluid consists of two layers with equal thicknesses $H/2$ and unequal densities ρ_1 on top and ρ_2 below, on the beta plane ($\beta_0 \neq 0$) over a flat bottom (at $z=0$) and under a rigid lid (at $z=H$, constant). The fluid is further assumed to be inviscid ($\mathcal{A}$ and $\nu_E = 0$). The basic flow is taken uniform in the horizontal and unidirectional but with distinct velocities in each layer:

$$\bar{u}_1 = U_1, \quad \bar{v}_1 = 0 \quad \text{for} \quad \frac{H}{2} \leq z \leq H \tag{17.27a}$$

$$\bar{u}_2 = U_2, \quad \bar{v}_2 = 0 \quad \text{for} \quad 0 \leq z \leq \frac{H}{2}. \tag{17.27b}$$

As we shall see, it is precisely the velocity difference $\Delta U = U_1 - U_2$ between the two layers, the vertical shear, that causes the instability. For simplicity, the dynamics are chosen to be quasi-geostrophic, prompting us to introduce a streamfunction ψ and potential vorticity q that obey (16.16) and (16.17):

$$\frac{\partial q}{\partial t} + J(\psi, q) = 0, \tag{17.28a}$$

$$q = \nabla^2 \psi + \frac{f_0^2}{N^2} \frac{\partial^2 \psi}{\partial z^2} + \beta_0 y. \tag{17.28b}$$

Because of identical layer thicknesses, the stratification frequency may be considered uniform, in agreement with the layered model of Section 12.2, where

equal layer heights corresponded to a uniform stratification. The second equation contains derivatives in z, which must be "discretized" to conform with a two-layer representation. For this, we place values ψ_1 and ψ_2 at midlevel in each layer and two additional values ψ_0 and ψ_3 above and below at equal distances (Fig. 17.6). These latter values fall beyond the boundaries and are defined for the sole purpose of enforcing boundary conditions in the vertical. The flat bottom and rigid lid require zero vertical velocity at those levels, which by virtue of (16.18e) translate into $\partial\psi/\partial z = 0$. In discretized form, the boundary conditions are $\psi_0 = \psi_1$ and $\psi_3 = \psi_2$. The second derivatives may then be approximated as

$$\left.\frac{\partial^2\psi}{\partial z^2}\right|_1 \approx \frac{\psi_0 - 2\psi_1 + \psi_2}{\Delta z^2} = \frac{\psi_1 - 2\psi_1 + \psi_2}{(H/2)^2} = \frac{4(\psi_2 - \psi_1)}{H^2}$$
$$\left.\frac{\partial^2\psi}{\partial z^2}\right|_2 \approx \frac{\psi_1 - 2\psi_2 + \psi_3}{\Delta z^2} = \frac{\psi_1 - 2\psi_2 + \psi_2}{(H/2)^2} = \frac{4(\psi_1 - \psi_2)}{H^2}.$$

In a similar vein, we discretize the stratification frequency:

$$N^2 = -\frac{g}{\rho_0}\frac{d\rho}{dz} \approx -\frac{g}{\rho_0}\frac{\rho_1 - \rho_2}{\Delta z} = +\frac{2g(\rho_2 - \rho_1)}{\rho_0 H} = \frac{2g'}{H}, \tag{17.29}$$

for which we have defined the reduced gravity $g' = g(\rho_2 - \rho_1)/\rho_0$. It is also convenient to introduce the baroclinic radius of deformation as

$$R = \frac{1}{f_0}\sqrt{g'\frac{H_1 H_2}{H_1 + H_2}} = \frac{\sqrt{g'H}}{2f_0}. \tag{17.30}$$

The set of two governing equations can now be written as follows:

$$\frac{\partial q_1}{\partial t} + J(\psi_1, q_1) = 0 \tag{17.31a}$$
$$\frac{\partial q_2}{\partial t} + J(\psi_2, q_2) = 0, \tag{17.31b}$$

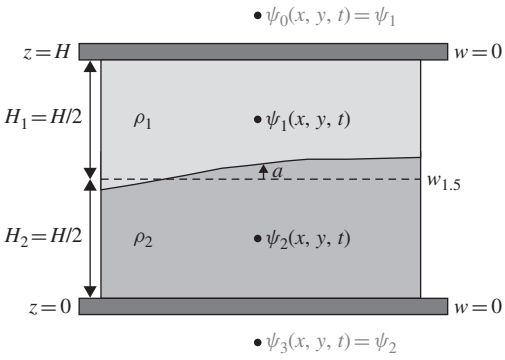

FIGURE 17.6 Representation of the vertical stratification by two layers of uniform density in a quasi-geostrophic model.

where the potential vorticities q_1 and q_2 are expressed in terms of the streamfunctions ψ_1 and ψ_2 as

$$q_1 = \nabla^2\psi_1 + \frac{1}{2R^2}(\psi_2 - \psi_1) + \beta_0 y \tag{17.32a}$$

$$q_2 = \nabla^2\psi_2 - \frac{1}{2R^2}(\psi_2 - \psi_1) + \beta_0 y. \tag{17.32b}$$

From these quantities, the primary physical variables are derived as follows [see Eqs. (16.18)]

$$u_i = -\frac{\partial\psi_i}{\partial y}, \quad v_i = +\frac{\partial\psi_i}{\partial x} \tag{17.33a}$$

$$w_{1.5} = \frac{2f_0}{N^2 H}\left[\frac{\partial(\psi_2 - \psi_1)}{\partial t} + J(\psi_1, \psi_2)\right] \tag{17.33b}$$

$$p_i' = \rho_0 f_0 \psi_i, \tag{17.33c}$$

where $i = 1, 2$. The vertical displacement a of the density interface between the layers can be obtained from the hydrostatic balance $p_2' = p_1' + (\rho_2 - \rho_1)ga$, which in terms of the streamfunctions yields

$$a = \frac{f_0}{g'}(\psi_2 - \psi_1). \tag{17.34}$$

The same set of equations can be derived from the two-layer model of Section 12.4, in which the quasi-geostrophic approach is applied in each layer, following the perturbation technique of Chapter 16.

The basic-state values of ψ_i and q_i corresponding to (17.27) are

$$\bar{\psi}_1 = -U_1 y, \quad \bar{q}_1 = \left(\beta_0 + \frac{\Delta U}{2R^2}\right) y \tag{17.35a}$$

$$\bar{\psi}_2 = -U_2 y, \quad \bar{q}_2 = \left(\beta_0 - \frac{\Delta U}{2R^2}\right) y. \tag{17.35b}$$

Adding a perturbation ψ_i' to $\bar{\psi}_i$ with corresponding perturbation q_i' to $\bar{q}_i$, both of infinitesimal amplitudes so that the equations can be linearized, we obtain, from (17.31) and (17.32), the following:

$$\frac{\partial q_i'}{\partial t} + J(\bar{\psi}_i, q_i') + J(\psi_i', \bar{q}_i) = 0 \tag{17.36a}$$

$$q_1' = \nabla^2\psi_1' + \frac{1}{2R^2}\left(\psi_2' - \psi_1'\right) \tag{17.36b}$$

$$q_2' = \nabla^2\psi_2' - \frac{1}{2R^2}\left(\psi_2' - \psi_1'\right). \tag{17.36c}$$

Elimination of q' and replacement of the basic-flow quantities with (17.35) yield a pair of coupled equations for ψ_1' and ψ_2':

$$\left(\frac{\partial}{\partial t}+U_1\frac{\partial}{\partial x}\right)\left[\nabla^2\psi_1'+\frac{1}{2R^2}(\psi_2'-\psi_1')\right]+\left(\beta_0+\frac{\Delta U}{2R^2}\right)\frac{\partial\psi_1'}{\partial x}=0, \quad (17.37a)$$

$$\left(\frac{\partial}{\partial t}+U_2\frac{\partial}{\partial x}\right)\left[\nabla^2\psi_2'-\frac{1}{2R^2}(\psi_2'-\psi_1')\right]+\left(\beta_0-\frac{\Delta U}{2R^2}\right)\frac{\partial\psi_2'}{\partial x}=0. \quad (17.37b)$$

Because both these equations have coefficients independent of x, y, and time, a sinusoidal function in those variables is a solution, and we write

$$\psi_i'=\Re\left[\phi_i e^{\mathrm{i}(k_x x+k_y y-\omega t)}\right], \quad (17.38)$$

where ϕ_1 and ϕ_2 form a pair of unknowns giving the vertical structure of the wave perturbation, k_x and k_y are horizontal wavenumber components (both taken as real), and ω is the angular frequency. The symbol $\Re$ indicates that only the real part of what follows is retained. Should the frequency ω be complex with a positive imaginary part, exponential growth occurs in time, and the wave is unstable. Substitution in (17.37) leads to algebraic equations for ϕ_1 and ϕ_2:

$$(U_1-c)\left[-k^2\phi_1+\frac{1}{2R^2}(\phi_2-\phi_1)\right]+\left(\beta_0+\frac{\Delta U}{2R^2}\right)\phi_1=0 \quad (17.39a)$$

$$(U_2-c)\left[-k^2\phi_2-\frac{1}{2R^2}(\phi_2-\phi_1)\right]+\left(\beta_0-\frac{\Delta U}{2R^2}\right)\phi_2=0, \quad (17.39b)$$

in which we have defined $c=\omega/k_x$ and $k^2=k_x^2+k_y^2$. At this point, it is useful to decompose the ϕ values into barotropic and baroclinic components:

$$\text{Barotropic component:} \quad A=\frac{\phi_1+\phi_2}{2} \quad (17.40a)$$

$$\text{Baroclinic component:} \quad B=\frac{\phi_1-\phi_2}{2}. \quad (17.40b)$$

The sum and difference of the preceding equations then yield

$$\left[2\beta_0-k^2(U_1+U_2-2c)\right]A-k^2\Delta U B=0 \quad (17.41a)$$

$$\left(\frac{1}{R^2}-k^2\right)\Delta U A+\left[2\beta_0-\left(k^2+\frac{1}{R^2}\right)(U_1+U_2-2c)\right]B=0. \quad (17.41b)$$

Note that a purely barotropic solution ($B=0$, $A\neq 0$) is possible only in the absence of shear ($\Delta U=0$), and for a wave speed $c=U-\beta_0/k^2$ easily interpreted as a barotropic planetary wave.

The preceding two equations form a homogeneous system of coupled linear equations for the constants A and B, the solution of which is trivially $A=B=0$ unless the determinant of the system vanishes. This occurs when

$$R^2k^2(1+R^2k^2)\left(\frac{U_1+U_2-2c}{\Delta U}\right)^2-2\frac{\beta_0R^2}{\Delta U}(1+2R^2k^2)\left(\frac{U_1+U_2-2c}{\Delta U}\right)+4\frac{\beta_0^2R^4}{\Delta U^2}+R^2k^2(1-R^2k^2)=0, \quad (17.42)$$

the c solution of which can be expressed as

$$\frac{U_1+U_2-2c}{\Delta U}=\frac{\beta_0R^2}{\Delta U}\frac{2R^2k^2+1}{R^2k^2(R^2k^2+1)}\pm\frac{1}{R^2k^2(R^2k^2+1)}\sqrt{\frac{\beta_0^2R^4}{\Delta U^2}-R^4k^4(1-R^4k^4)}. \quad (17.43)$$

It is clear from this equation that the phase speed c of the wave is real as long as the quantity under the square root is positive, that is, as long as the wavenumber k satisfies the condition

$$R^4k^4(1-R^4k^4)\le\left(\frac{\beta_0R^2}{\Delta U}\right)^2. \quad (17.44)$$

The function $R^4k^4(1-R^4k^4)$ reaches a maximum of $1/4$ for $Rk=1/2^{1/4}=0.841$ (Fig. 17.7), and therefore, the condition is met for a perturbation of any wavenumber as long as

$$|\Delta U|\le 2\beta_0R^2=\frac{\beta_0g'H}{2f_0^2}. \quad (17.45)$$

In other words, the system is stable to all small perturbations when the velocity shear ΔU is sufficiently weak not to exceed $2\beta_0R^2$. Put another way, shear is destabilizing because the greater is ΔU, the higher is the likelihood that the threshold value will be exceeded. In contrast, the beta effect is stabilizing because the greater is β_0, the more generous is the threshold.

When the velocity shear exceeds the threshold value, condition (17.45) is not met, and not all wavenumbers satisfy condition (17.44). Perturbations of wavenumber $k=\sqrt{k_x^2+k_y^2}$ within the interval $k_{\min}<k<k_{\max}$ are unstable,

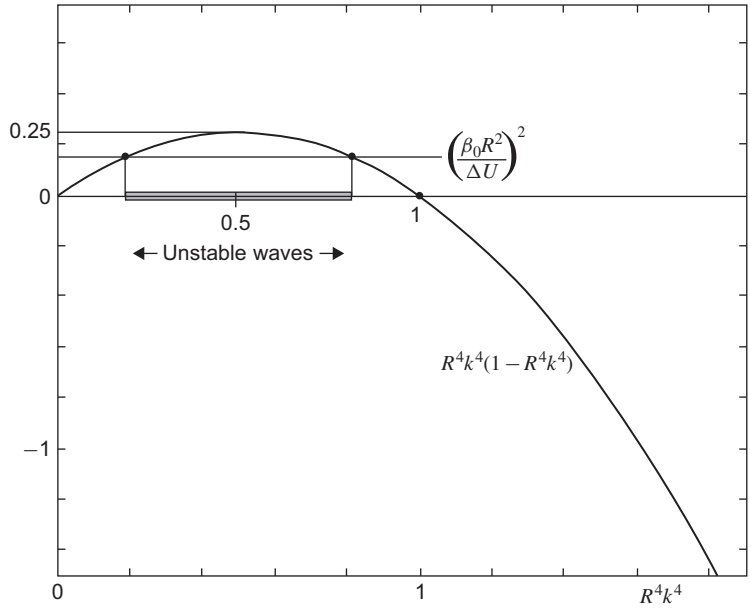

FIGURE 17.7 Instability interval for two-layer baroclinic instability. Small-amplitude waves with wavenumber k falling in the hatched interval are unstable and grow in time.

where

$$k_{\min} = \left(\frac{1 - \sqrt{1 - 4\beta_0^2 R^4 / \Delta U^2}}{2R^4} \right)^{1/4} \tag{17.46a}$$

$$k_{\max} = \left(\frac{1 + \sqrt{1 - 4\beta_0^2 R^4 / \Delta U^2}}{2R^4} \right)^{1/4} . \tag{17.46b}$$

Note that unstable waves not only grow but also propagate in time. According to (17.43), the real part of the wave speed is

$$\Re(c) = \frac{U_1 + U_2}{2} - \frac{\beta_0}{2k^2} \frac{1 + 2R^2k^2}{1 + R^2k^2} \tag{17.47}$$

when c is complex, and thus, the zonal propagation speed is $(U_1 + U_2)/2$, or the average velocity of the basic flow, minus a (westward) planetary wave speed.

From Fig. 17.7 or from Eq. (17.45), we see that instability on the beta plane can only occur for a sufficiently large shear ΔU. With increasing ΔU starting

from a stable flow, the first instability occurs when $\Delta U = 2\beta_0 R^2$. At this level of shear, the wavenumber of the sole unstable mode is $k = 1/(2^{1/4}R) = 0.841/R$ and has the wavelength

$$\lambda = \frac{2\pi}{k} = 7.472\ R. \tag{17.48}$$

For a given $\Delta U > 2\beta_0 R^2$, a range of wavelengths and wavenumbers ($k_{\min} < k < k_{\max}$) correspond to unstable waves, and wavelength (17.48) happens not to be that of the fastest growing wave.

Finding the fastest growing wave is rather complicated with a nonzero beta effect. To keep the analysis to a minimum, we thus restrict our attention to the f-plane ($\beta_0 = 0$, leading to $k_{\min} = 0$ and $k_{\max} = 1/R$), which can be justified when considering shorter scales, more typical of the ocean than of the atmosphere. All perturbations of wavenumber $k < 1/R$ are unstable, corresponding to all wavelengths longer than $2\pi R$. Until finite-amplitude effects become important, the perturbation that distorts the system most—and thus the one most noticeable at the start of the instability—is the one with the largest growth rate, ω_i (the imaginary part of ω). On the f-plane, Eq. (17.43) gives $c = c_r + \mathrm{i}\, c_i$ with real part $c_r = (U_1 + U_2)/2$ and positive imaginary part

$$c_i = \frac{\Delta U}{2}\sqrt{\frac{1 - k^2R^2}{1 + k^2R^2}} \qquad (kR < 1) \tag{17.49}$$

The growth rate is $\omega_i = k_x c_i$ and reaches a maximum with respect to k_x and k_y for

$$k_x = \frac{\sqrt{\sqrt{2} - 1}}{R} = \frac{0.644}{R}, \qquad k_y = 0. \tag{17.50}$$

The wavelength of the fastest growing mode is $\lambda = 9.763\ R$.

It is interesting at this point to return to our initial considerations (Section 17.3) and to confirm them with the preceding solution. First and foremost, the fact that both the critical wavelength for instability ($2\pi R$) and the wavelength of the fastest growing perturbation ($9.763\ R$) are proportional to R validates the argument that self-amplification requires a scale on the order of the deformation radius. Physically, it also verifies that the instability process involves a rearrangement of potential vorticity between relative vorticity and vertical stretching.

The necessary phase relationship between the transverse displacements of the upper and lower fluids can be checked as follows. We define the transverse displacement d, one for each layer, in terms of the meridional velocity by

$$v' = \frac{\partial d}{\partial t} + \bar{u}\,\frac{\partial d}{\partial x}, \tag{17.51}$$

after linearization. Expressing v' in terms of the streamfunction perturbation ($v' = \partial\psi'/\partial x$) and implementing the wave form $d_i = \Re[D_i \exp \mathrm{i}\,(k_x x + k_y y - \omega t)]$, we then obtain

$$D_i = \frac{\phi_i}{U_i - c}, \tag{17.52}$$

from which we can deduce the ratio of transverse displacements in the upper and lower layers:

$$\frac{D_1}{D_2} = \frac{U_2 - c}{U_1 - c}\,\frac{A+B}{A-B}. \tag{17.53}$$

For the fastest growing wave on the f-plane in the case $U_1 > U_2$ (i.e., $\Delta U > 0$), the wavenumber is $k = 0.644/R$, and the ratio of displacements is found to be

$$\begin{aligned}\frac{D_1}{D_2} &= 0.66 - \mathrm{i}0.75 \\ &= \cos(49^\circ) + \mathrm{i}\sin(-49^\circ).\end{aligned} \tag{17.54}$$

Physically, the negative 49° angle corresponds to an advance (in the direction of the basic flow) of the top displacement over that in the bottom layer. The shift is not the 90° phase quadrature that was expected, but it is in the direction anticipated from the simple physical argument of the previous section.

From an observational point of view, however, the interest lies in the pressure field, which is proportional to the streamfunction [see (17.33c)]. Within an arbitrary multiplicative constant, which the linear theory is unable to determine, the pressure field associated with the fastest growing perturbation can be expressed in terms of the vertical structure of the streamfunction perturbation:

$$\begin{aligned}\frac{\phi_1}{\phi_2} &= \frac{A+B}{A-B} \\ &= \cos(66^\circ) + \mathrm{i}\sin(66^\circ).\end{aligned} \tag{17.55}$$

From this, we conclude that the crests and troughs of the pressure pattern at the top lag those of the bottom pattern by a fifth to sixth of a wavelength.

Finally, the maximum growth rate is

$$\omega_i = k_x c_i = \frac{\Delta U}{R}\,\frac{\sqrt{2}-1}{2}. \tag{17.56}$$

If we assume the Rossby number Ro to be small, which must be by virtue of the quasi-geostrophic approximation, we find $\omega_i \lesssim 0.2 f Ro \ll f$. The timescale characteristic of the growth is therefore much longer than f^{-1} so that the solution is consistent within the quasi-geostrophic theory.

To conclude we briefly examine the confining effect of boundaries, taken as vertical walls at $y = 0$ and $y = L$. The basic flow, in the x-direction, satisfies the

impermeability condition and needs no adjustment. As for the perturbation flow, the normal velocity must vanish at each boundary, which according to (17.33a) demands $\partial\psi/\partial x = 0$ at $y = 0$ and $y = L$. With ψ given by (17.38), both boundary conditions can be simultaneously met only when the sinusoidal structure in y of the streamfunction is such that $k_y L = n\pi$ with $n = 1, 2, \ldots$. In this case

$$k^2 R^2 = \left(k_x^2 + \frac{n^2\pi^2}{L^2}\right) R^2. \tag{17.57}$$

Since according to (17.46), instability is only possible for $k^2R^2 < 1$, the boundaries must be sufficiently distant from each other to satisfy

$$\frac{R^2}{L^2} \leq \frac{1}{\pi^2}. \tag{17.58}$$

This simply means that the domain must be wide enough to accommodate the instability, otherwise it cannot develop.

Interestingly, the preceding inequality, (17.58), shows that the Burger number associated with the basic flow of width L should not exceed 0.1, and this implies, according to (16.34), that the energy in the basic flow must be predominantly in the form of available potential energy in the basic flow. This reserve of potential energy feeds the growth of the instability. Note that, for the perturbation itself, the Burger number is always on the order of one, since the scale of the instability is the deformation radius.

17.5 HEAT TRANSPORT

The qualitative arguments developed in Section 17.3 revolved around the idea that if a flow in thermal-wind equilibrium is unstable, it will seek a lower level of energy by relaxation of density surfaces toward simple gravitational equilibrium. If we now think of the atmosphere, where the heavier fluid is colder air and the lighter fluid warmer air, relaxation implies a flow of warm air spilling over the colder air ($+y$-direction in Fig. 17.4) and of cold air intruding under the warmer air ($-y$-direction in Fig. 17.4). In other words, we expect a net heat flux and, because the atmospheric temperature typically increases toward the equator, a poleward heat flux. Let us examine what the preceding linear theory predicts.

The vertically integrated heat flux in the north-south direction (y-direction) per unit length of east-west direction (x-direction) is defined as

$$q = \rho_0 C_p \int_0^H \overline{vT}\, \mathrm{d}z, \tag{17.59}$$

where C_p is the heat capacity of the fluid at constant pressure (1005 $\mathrm{J\,kg^{-1}\,K^{-1}}$ for dry air, 4186 $\mathrm{J\,kg^{-1}\,K^{-1}}$ for seawater), T is temperature, and the overbar

indicates an average over a wavelength in the x-direction. In the two-layer representation of Fig. 17.6, the vertical integration is straightforward:

$$\begin{aligned} q &= \rho_0 C_p \left[\overline{v_2 T_2 (H_2 + a)} + \overline{v_1 T_1 (H_1 - a)} \right] \\ &= \rho_0 C_p \left[\overline{v_2 a}\, T_2 - \overline{v_1 a}\, T_1 \right] \end{aligned} \tag{17.60}$$

since the temperature is uniform within each layer and the integral over a wavelength yields $\overline{v_1} = 0$ and $\overline{v_2} = 0$. Using $v_i = v_i' = \partial \psi_i'/\partial x$ and $a = f_0(\psi_2' - \psi_1')/g'$ and then exploiting $\overline{\partial \psi_i^2/\partial x} = 0$ and $\overline{\partial(\psi_2 \psi_1)/\partial x} = 0$, we have successively

$$\begin{aligned} q &= \frac{\rho_0 C_p f_0}{g'} \left[T_2 \overline{\frac{\partial \psi_2'}{\partial x}(\psi_2' - \psi_1')} - T_1 \overline{\frac{\partial \psi_1'}{\partial x}(\psi_2' - \psi_1')} \right] \\ &= \frac{\rho_0 C_p f_0}{g'} \left[-T_2 \overline{\psi_1' \frac{\partial \psi_2'}{\partial x}} - T_1 \overline{\psi_2' \frac{\partial \psi_1'}{\partial x}} \right] \\ &= \frac{\rho_0 C_p f_0}{g'} (T_1 - T_2) \overline{\psi_1' \frac{\partial \psi_2'}{\partial x}}. \end{aligned} \tag{17.61}$$

Some rather lengthy algebra using the periodic structure (17.38) and the modal decomposition (17.40) successively provides

$$\begin{aligned} \overline{\psi_1' \frac{\partial \psi_2'}{\partial x}} &= \frac{k_x}{2} [\Im(\phi_1)\Re(\phi_2) - \Re(\phi_1)\Im(\phi_2)] e^{2\Im(\omega)t} \\ &= k_x \left[\Re(A)\Im(B) - \Im(A)\Re(B) \right] e^{2\Im(\omega)t}. \end{aligned}$$

The real and imaginary parts of Eq. (17.41a) are

$$\begin{aligned} \left[2\beta_0 - k^2 (U_1 + U_2 - 2c_r) \right] \Re(A) - k^2 c_i \Im(A) &= k^2 \Delta U \Re(B) \\ \left[2\beta_0 - k^2 (U_1 + U_2 - 2c_r) \right] \Im(A) + k^2 c_i \Re(A) &= k^2 \Delta U \Im(B), \end{aligned}$$

where c_r and c_i stand, respectively, for the real and imaginary parts of c. From these relations, it follows that

$$\Re(A)\Im(B) - \Im(A)\Re(B) = \frac{c_i}{\Delta U} |A|^2. \tag{17.62}$$

Putting it altogether, we finally obtain an expression for the heat flux

$$q = \frac{\rho_0 C_p f_0 \Im(\omega)}{g' \Delta U} (T_1 - T_2) |A|^2 e^{2\Im(\omega)t}. \tag{17.63}$$

It is clear from this expression that the heat flux is nonzero only when the wave is unstable (imaginary part of $\omega \neq 0$) and is positive, as anticipated by the earlier physical arguments. In the atmospheric case, this means that the heat flux is poleward.

Because the earth is heated in the tropics and cooled at high latitudes, the global heat budget requires a net poleward heat flux in each hemisphere. The flux is carried by both atmosphere and ocean. In the atmosphere, higher temperatures in the tropics and lower temperatures at high latitudes maintain an overall thermal wind system, which is baroclinically unstable. Vortices emerge on the scale of the baroclinic radius of deformation ($R \sim 1000$ km), which carry the heat poleward and tend to relax the thermal-wind structure. The latter, however, is maintained by continuous heating in the tropics and cooling at high latitudes. As a consequence, the cyclones and anticyclones of our weather are the primary agents of meridional heat transfer in the atmosphere. Without baroclinic instability, they would not exist, and weather forecasting would be a much simpler task, but the tropical regions would be much hotter and the polar regions, much colder. Also, the dominance of zonal winds would preclude efficient mixing across latitudes, exacerbating certain problems by severely limiting, for example, the spread of volcanic ash. Moreover, less atmospheric variability would imply greatly reduced temperature and moisture contrasts and thus much less precipitation at midlatitudes. All in all, we must concede that baroclinic instability in our atmosphere is highly beneficial.

In the ocean, the situation is quite different. The presence of meridional boundaries prevents thermal-wind type currents from encircling the globe, and ocean circulation consists of large-scale gyres (Chapter 20). The meridional branches of these gyres, especially the western boundary currents (Gulf Stream in the North Atlantic, Kuroshio in North Pacific), are the main conveyers of heat toward high latitudes (e.g., Siedler, Church & Gould, 2001). This greatly reduces the need for poleward heat transfer by eddies. Baroclinic instability is active in regions of strong currents, such as the Antarctic Circumpolar Current, Gulf Stream, and Kuroshio extensions, but the eddies so created transport little net heat across latitudes. One should also remember here that the baroclinic radius of deformation is significantly shorter in the ocean than in the atmosphere, with the consequence that the aggregate effect of eddies in the ocean is more regional than planetary.

17.6 BULK CRITERIA

The theory exposed in Section 17.4 is admittedly a very simplified version of baroclinic-instability physics. Since it is not our purpose here to review the many advanced analyses that have been published over the years since the pioneering studies of Charney, Eady, and Phillips (the interested reader will find a survey in the book of Pedlosky, 1987), we will once again turn to integral relations, from which some necessary but not sufficient criteria for instability can be derived. We already used this approach in the study of horizontally sheared currents in homogeneous fluids (Section 10.2) and of vertically sheared currents in nonrotating stratified fluids (Section 14.2). Although a general presentation that would encompass the preceding two situations and baroclinic instability could

be formulated, it is most instructive to emphasize the conditions necessary for baroclinic instability by basing the analysis on the quasi-geostrophic equation.[5] The following derivations are based on the work of Charney and Stern (1962).

We start again with Eqs. (17.28) but this time retain continuous variation in the vertical albeit with uniform stratification frequency. Adding a small perturbation to a basic zonal flow $\bar{u}(y,z)$ possessing both horizontal and vertical shear, we obtain

$$\frac{\partial q'}{\partial t} + J(\bar{\psi}, q') + J(\psi', \bar{q}) = 0 \tag{17.64a}$$

$$q' = \nabla^2 \psi' + \frac{f_0^2}{N^2} \frac{\partial^2 \psi'}{\partial z^2}, \tag{17.64b}$$

where $\bar{\psi}(y,z)$ is the streamfunction associated with the basic zonal flow ($\bar{u} = -\partial \bar{\psi}/\partial y$), and the basic potential vorticity is related to it by

$$\bar{q} = \frac{\partial^2 \bar{\psi}}{\partial y^2} + \frac{f_0^2}{N^2} \frac{\partial^2 \bar{\psi}}{\partial z^2} + \beta_0 y. \tag{17.65}$$

Substitution of (17.64b) and (17.65) into (17.64a) yields a single equation for the streamfunction perturbation ψ', which includes nonconstant coefficients depending on the basic flow structure via $\bar{\psi}$ and $\bar{q}$. Because those coefficients depend only on y and z, a waveform solution in x and time can be sought: $\psi'(x,y,z,t) = \Re[\phi(y,z)\exp(\mathrm{i}k_x(x-ct))]$. The amplitude function $\phi(y,z)$ must obey

$$\frac{\partial^2 \phi}{\partial y^2} + \frac{f_0^2}{N^2} \frac{\partial^2 \phi}{\partial z^2} + \left(\frac{1}{\bar{u}-c} \frac{\partial \bar{q}}{\partial y} - k_x^2 \right) \phi = 0, \tag{17.66}$$

with $\bar{q}$ defined in (17.65).

The upper and lower boundaries are once again taken as rigid horizontal surfaces, where the vertical velocity must vanish. According to (16.18e), this implies after splitting between basic flow and perturbation and linearizing:

$$(\bar{u}-c)\frac{\partial \phi}{\partial z} - \frac{\partial \bar{u}}{\partial z}\phi = 0 \quad \text{at} \quad z = 0, H. \tag{17.67}$$

In the meridional direction, we idealize the domain to a channel of width L between two vertical walls, where the meridional velocity $v' = \partial \psi'/\partial x$ vanishes. We thus impose

$$\phi = 0 \quad \text{at} \quad y = 0,\ L. \tag{17.68}$$

[5] Actually, this equation eliminates the Kelvin–Helmholtz instability but not barotropic instability.

Multiplying (17.66) by the complex conjugate ϕ^* of ϕ, integrating over the meridional and vertical extents of the domain, performing integrations by parts, and using the preceding boundary conditions, we obtain

$$\int_0^H \int_0^L \left[\left| \frac{\partial \phi}{\partial y} \right|^2 + \frac{f_0^2}{N^2} \left| \frac{\partial \phi}{\partial z} \right|^2 + k_x^2 |\phi|^2 \right] \mathrm{d}y\,\mathrm{d}z$$
$$= \int_0^H \int_0^L \frac{1}{\bar{u}-c} \frac{\partial \bar{q}}{\partial y} |\phi|^2 \,\mathrm{d}y\,\mathrm{d}z$$
$$+ \int_0^L \left[\frac{f_0^2}{N^2} \frac{1}{\bar{u}-c} \frac{\partial \bar{u}}{\partial z} |\phi|^2 \right]_0^H \mathrm{d}y. \tag{17.69}$$

The imaginary part of this equation is

$$c_i \left\{ \int_0^H \int_0^L \frac{|\phi|^2}{|\bar{u}-c|^2} \frac{\partial \bar{q}}{\partial y} \,\mathrm{d}y\,\mathrm{d}z + \int_0^L \left[\frac{f_0^2}{N^2} \frac{|\phi|^2}{|\bar{u}-c|^2} \frac{\partial \bar{u}}{\partial z} \right]_0^H \mathrm{d}y \right\} = 0. \tag{17.70}$$

A necessary condition for instability is that c_i not be zero (so that the disturbance grows in time). According to (17.70), this implies that the quantity within braces must vanish, and therefore conditions for instability are

1. $\partial \bar{q}/\partial y$ changes sign in the domain, or
2. the sign of $\partial \bar{q}/\partial y$ is opposite to that of $\partial \bar{u}/\partial z$ at the top, or
3. the sign of $\partial \bar{q}/\partial y$ is the same as that of $\partial \bar{u}/\partial z$ at the bottom.

A sufficient condition for stability is that none of the above three conditions is met.

Before proceeding, it is worth applying this result to the case of a uniform shear flow $\bar{u} = Uz/H$ in the absence of the beta effect ($\beta_0 = 0$). We then have $\bar{q} = 0$ and $\partial \bar{u}/\partial z = U/H$, reducing (17.70) to

$$c_i \int_0^L \frac{f_0^2 U}{N^2 H} \left[\frac{|\phi(y,H)|^2}{|U-c|^2} - \frac{|\phi(y,0)|^2}{|c|^2} \right] \mathrm{d}y = 0, \tag{17.71}$$

in which the integral is obviously not sign definite. Stability cannot be guaranteed, and this flow is unstable (Eady, 1949). Had we instead chosen a weak flow field with no vertical shear at the boundaries [e.g., $\bar{u}(z) = U(3z^2/H^2 - 2z^3/H^3)$] and on the beta plane ($\partial \bar{q}/\partial y \simeq \beta_0$), we would have concluded (after much lengthier mathematics) that this flow is stable to all perturbations. This points to the sensitivity of baroclinic instability to the structure of the basic flow field.

Another application of (17.70) is to laterally sheared but vertically uniform flow, $\bar{u}(y)$. Then, the potential-vorticity gradient is $\mathrm{d}\bar{q}/\mathrm{d}y = \beta_0 - \mathrm{d}^2\bar{u}/\mathrm{d}y^2$, and

(17.70) reduces to

$$c_i \left[H \int_0^L \frac{|\phi|^2}{|\bar{u}-c|^2} \left(\beta_0 - \frac{\mathrm{d}^2 \bar{u}}{\mathrm{d}y^2} \right) \mathrm{d}y \right] = 0. \tag{17.72}$$

Here, we recover the result of barotropic instability obtained in Section 10.2 [see Eq. (10.13)] and conclude that the instability conditions stated above include both barotropic and baroclinic instability criteria. Put another way, barotropic and baroclinic instabilities are two end members of a more general barotropic–baroclinic mixed instability.

Charney and Stern (1962) explored the case when $\partial \bar{u}/\partial z$ vanishes at both upper and lower boundaries by assuming a vanishing thermal-wind there (e.g., uniform temperature) and/or taking the limits $H \to \infty$, $\bar{u}(H) \to 0$. Of (17.70), only the first integral remains, and the necessary condition for instability is that $\partial \bar{q}/\partial y$ vanishes somewhere in the domain, a statement identical in form to—but differing in content from—the barotropic-instability criterion of Section 10.2.

According to Gill et al. (1974), the presence of a bottom slope in the meridional direction modifies the last of the three conditions as follows:

3. The sign of $\partial \bar{q}/\partial y$ is the same as that of $\partial \bar{u}/\partial z - (N^2/f_0)\mathrm{d}b/\mathrm{d}y$ at the bottom $z = b(y)$.

Therefore, a bottom slope may be either stabilizing or destabilizing. It is generally a stabilizing factor if it creates an ambient potential-vorticity gradient in the same direction as the beta effect (i.e., shallower fluid toward higher latitudes; see Fig. 9.6) and a destabilizing factor otherwise. However, the theory fails to take into account the zonal topographic gradients that are more common on Earth (e.g., the Rocky Mountains in North America for the atmosphere and the Mid-Atlantic Ridge along the North Atlantic for the ocean).

There exist a number of other studies in baroclinic instability. The interested reader is referred to Gill (1982, Chapter 13), Pedlosky (1987, Chapter 7), and Vallis (2006, Chapters 6 and 9).

17.7 FINITE-AMPLITUDE DEVELOPMENT

Once the instability is underway, exponential growth eventually leads to perturbations whose amplitudes are no longer small compared to the size of the basic flow. Linear theory then ceases to be valid, and we must deal with the nonlinear equations, resorting as usual to numerical methods. The task in front of us is solving Eqs. (17.32) and (17.31) using the quasi-geostrophic approximation. Since these equations are similar to those of the two-dimensional QG model of Section 16.7, we may start with the discretization of the latter and adapt it for our present purpose. In addition, for the study of baroclinic instability, it is useful to exploit the fact that, because the basic flow is stationary, only the

perturbation variables need to be updated. So, we solve

$$\frac{\partial q_1'}{\partial t} + J(\psi_1, q_1) = 0, \tag{17.73a}$$

$$\frac{\partial q_2'}{\partial t} + J(\psi_2, q_2) = 0. \tag{17.73b}$$

Note that the Jacobian operator J involves the streamfunction and potential vorticity of the flow consisting of both basic flow and perturbation. Updating only perturbation components, therefore, does not involve any linearization. Equations (17.73) are readily discretized if we use the Arakawa Jacobian of Section 16.7. For time stepping, the simplest approach is an explicit scheme such as the predictor-corrector method, so that we can easily calculate the potential vorticities at time level $n+1$ knowing both streamfunction and vorticity at time level n.

Once perturbations q_1' and q_2' are obtained at the new time level, we have to invert a pair of Poisson equations (17.36b) and (17.36c) to calculate the respective streamfunction at the same moment, in preparation of the next time step. Solving these Poisson equations, however, is more complicated than in the two-dimensional case of Chapter 16 because we are now in the presence of two coupled equations. To overcome the added complexity, we generalize the iterative Gauss–Seidel approach, working jointly on ψ_1' and ψ_2'. Omitting the $'$ and referring to an iteration by superscript $^{(k+1)}$, we iterate in tandem as follows:

$$\psi_1^{(k+1)} = \psi_1^{(k)} + \alpha \left[\nabla^2 \psi_1 - q_1 + \frac{(\psi_2^{(k)} - \psi_1^{(k)})}{2R^2} \right]$$

$$\psi_2^{(k+1)} = \psi_2^{(k)} + \alpha \left[\nabla^2 \psi_2 - q_2 - \frac{(\psi_2^{(k)} - \psi_1^{(k+1)})}{2R^2} \right].$$

The spatial operator ∇^2 is calculated using the most recent values of ψ available on the discrete grid, and the iterations are performed at a frozen time level.[6] The parameter α contains discretization constants and over-relaxation parameters. This approach is easily implemented and can be generalized to more than two layers.

For the present two-layer model, another option is to decouple the equations by decomposing q_1 and q_2 into their barotropic and baroclinic parts. The sum and difference of (17.73a) and (17.73b) then yield two uncoupled equations that can be solved independently, possibly with different iteration schemes.

Once the iterations have converged, the two perturbation streamfunctions are known at the new time level, and the total (basic flow + perturbation)

[6] Do not confuse the time index ^{n} with the iteration index $^{(k)}$.

streamfunction and potential vorticity can be evaluated. The Arakawa Jacobian is then recalculated, and the time stepping continued.

To initialize the whole procedure, it is sufficient to provide initial conditions on either vorticity or streamfunction. If the streamfunction is provided as the initial condition, initial potential vorticity can be deduced from the streamfunction by definitions (17.36b)–(17.36c), and time stepping can start. If vorticity is provided as the initial condition, we have to begin with a solution (inversion) of the Poisson equations before time stepping can begin.

We also have to provide adequate boundary conditions. In the x-direction, the length of the domain is dictated by the wavelength of the perturbation whose stability is being investigated. Periodic conditions are then readily applied to both streamfunction and vorticity. In the y-direction, we assume a channel configuration with zonal boundaries at $y=0$ and $y=L$. The condition of zero normal velocity forces the streamfunction to be uniform along each wall at a given moment. At $t=0$, the values of the constants are dictated by the initial condition of the still unperturbed flow. In analytical studies, these initial constants are then kept fixed over time. This is justified by the fact that the analytical streamfunction perturbation possesses a wave structure in the x-direction, which demands that the amplitude of the wave be zero on the boundary.

With the nonlinear equations, the situation is different because all we need to ensure is that the instantaneous streamfunction, combining basic flow and perturbation, is constant along the wall. The value of the constant, however, is allowed to change with time. The physical reason lies in the possibility that the interface between the two layers flattens out, in which case the cumulated flow across the channel weakens in each layer. The problem we face is similar to the one encountered in Section 7.7, where values of the streamfunction on the periphery of islands had to be determined depending on the flow evolution itself. For the correct and subtle way of specifying such boundary conditions in a quasi-geostrophic model, we refer to McWilliams (1977). Here, we follow the simpler approach of Phillips (1954), which is appropriate to our configuration. The original equation for the velocity component u in an isopycnal model can be cast as

$$\frac{\partial u}{\partial t}+\frac{1}{2}\frac{\partial u^2}{\partial x}+v\frac{\partial u}{\partial y}=fv-\frac{1}{\rho_0}\frac{\partial P}{\partial x}. \tag{17.74}$$

For simplicity, there is no need to indicate to which layer we refer because the same type of equation holds for each layer. We can integrate the preceding equation over the wavelength λ in the x-direction. By virtue of periodicity, the second term of the left-hand side as well as the second term of the right-hand side will not contribute to the integral. As long as the wall coincides with the same x-direction, impermeability requires $v=0$, and the third term of the left-hand side and the first term of the right-hand side vanish. All that remains is the integration of the first term, which must vanish on its own. In terms of the

streamfunction ($u = -\partial\psi/\partial y$), we have

$$\int_0^\lambda \frac{\partial^2 \psi}{\partial y \partial t}\,\mathrm{d}x = 0 \text{ on a wall parallel the } x\text{-axis.} \tag{17.75}$$

In conclusion, the constant value to be ascribed to the streamfunction along an impermeable boundary is to be obtained from (17.75).

The implementation of this new boundary condition can be shown for the boundary at $y = 0$. To determine the value of $\psi_{i,1} = C_1$ along the boundary at the new time step, we discretize Eq. (17.75) as

$$C_1^{n+1} = C_1^0 + \frac{1}{m}\sum_{i=1}^{m}\left(\psi_{i,2}^{n+1} - \psi_{i,2}^0\right) \tag{17.76}$$

in which the sum covers the grid points along the wall. Hence, the value to be prescribed along the boundary depends on the yet unknown values $\psi_{i,2}^{n+1}$ in the interior of the domain, themselves depending on the boundary conditions. This circular dependence can be resolved by wrapping the evaluation of constant C_1 into the iterations of the Poisson solver, updating ψ not only in the interior but also on the boundary during the Gauss–Seidel iterations.

If the Poisson solver is applied to the perturbation ψ' only, then the boundary condition formulation is simpler: the initial value of $\int_0^\lambda \partial\psi/\partial y\,\mathrm{d}x$ is fixed by the basic flow, and $\int_0^\lambda \partial\psi'/\partial y\,\mathrm{d}x$ must be held at zero at all times.

The outlined numerical algorithm was implemented in `baroclinic.m` and is now used to simulate baroclinic instability as presented in Section 17.3 extended into the nonlinear regime. We show results of such a model simulation at different moments of the evolution (Fig. 17.8). For simplicity, we take $U_2 = -U_1$, so that the linear perturbation theory predicts a wave that amplifies in place.

Initially, the evolution follows the theoretical prediction: The perturbation grows without displacement, maintaining the expected phase shift between layers. After a while, however, the perturbation reaches a mature stage when its amplitude is comparable to the strength of the basic flow. We are then in the nonlinear regime. Now, the phase shift between layers diminishes, and the interface between layers relaxes. Together these changes indicate a barotropization of the flow, (Fig. 17.9) that is, the two layers begin to act more and more as if they were making a single layer. This is confirmed by the structure of the potential vorticity, which becomes almost vertically uniform by the end of the simulation. We conclude that baroclinic instability releases available potential energy and uses it to spin eddies and to strengthen the barotropic component of the flow.

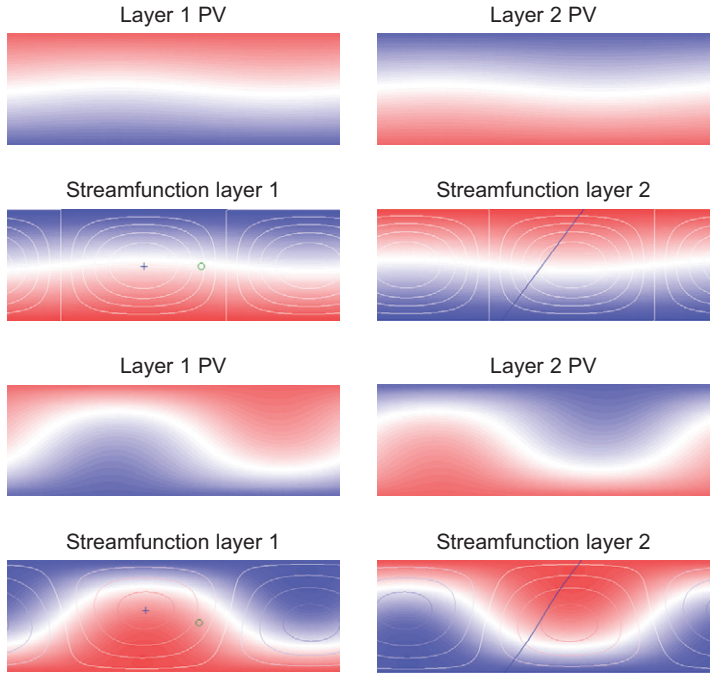

FIGURE 17.8 Evolution of a perturbed thermal wind. For each of the two snapshots during the evolution of the system, four panels show, in order of presentation: the upper layer potential vorticity, the lower layer potential vorticity, the upper layer streamfunction, and lower layer streamfunction. On the latter two, the contours depict the streamfunction perturbation. On the upper layer streamfunction plot, symbols have been added to represent the location of the maximum ψ' value of the upper (cross) and lower layer (circle). On the lower layer streamfunction plot, a line depicting the x-averaged position of the interface is shown. White separates the positive from negative values. For perturbations, the contoured values change over time. To view the evolution as computer animation, the reader should run `baroclinic.m` or look at the video provided with the files.

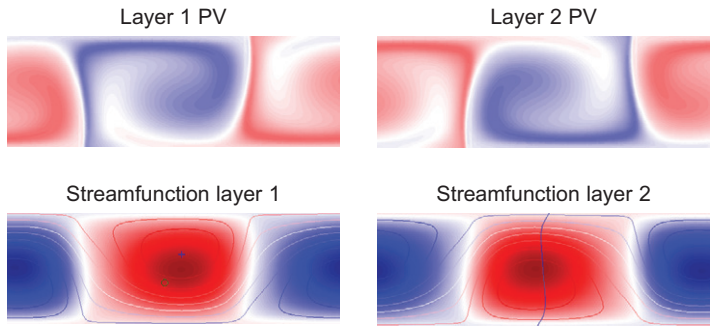

FIGURE 17.9 Further evolution of the instability showing barotropization of the flow.

ANALYTICAL PROBLEMS

17.1. Irrespectively of momentum considerations, suppose we exchange fluid parcels 1 and 2 of Fig. 17.10. Show that the potential energy released is maximum when the slope of the line connecting points 1 and 2 is half that of the isopycnal slope. Show that in this case, the release of potential energy per unit volume ΔPE is

$$\Delta PE = \frac{\rho_0}{4} N^2 L^2 \tag{17.77}$$

17.2. Demonstrate the assertion made at the end of Section 17.6 that the vertically sheared flow

$$\bar{u}(z) = U\left(3\,\frac{z^2}{H^2} - 2\,\frac{z^3}{H^3}\right)$$

in $0 \le z \le H$ is baroclinically stable on the beta plane as long as U falls below a critical value. What is that critical value?

17.3. Establish an energy budget involving quadratic forms of the perturbation variables. Then, derive an energy budget involving quadratic forms of the total velocity. Identify types of energy and the exchanges between them.

17.4. Compare the magnitudes of the potential and kinetic energies of the most unstable wave described in Section 17.4.

17.5. Assuming a general initial profile of the interface $a = \bar{a}(y)$, with zero total transport in each column, establish linearized equations a small perturbation of this situation must obey. Verify that for a linear interface, you retrieve formulation (17.37) with $U_1 = -U_2$.

17.6. Prove the assertion made at the end of Section 17.2 that the unstable regime of the wedge instability corresponds to particles moving along

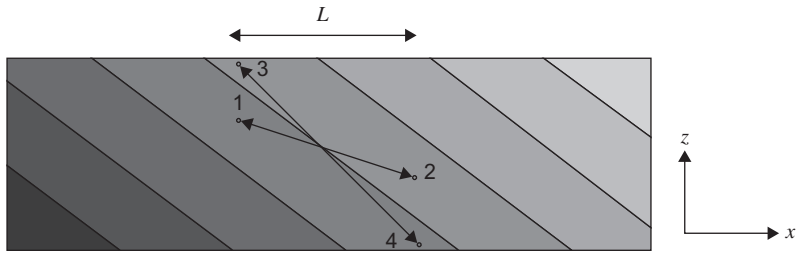

FIGURE 17.10 Exchange of fluid parcels across a system in thermal-wind balance. Exchange between parcels 1 and 2 leads to a release of potential energy, whereas exchange between parcels 3 and 4 would obviously lead to an increase in potential energy. Lighter shades represent lighter fluid.

surfaces wedged between geostrophic surfaces and isopycnals. (*Hint*: Solve for the equations of motion (17.14) for the vector displacement $(\Delta x, \Delta z)$ and study its direction.)

17.7. Apply the two-layer model of baroclinic instability to an atmospheric situation, where the domain height $H \sim 7$ km encompasses the troposphere with typical stratification $N = 10^{-2}\,\mathrm{s}^{-1}$. Calculate the wavelength of the most unstable mode. Compare to the weather patterns of the synoptic maps you see any day in the newspaper or online. Then, calculate the growth rate and compare to the lead time of a typical weather forecast.

NUMERICAL EXERCISES

17.1. Program (17.43) and plot, as a function of ΔU, the wavenumber corresponding to the maximum growth rate and the growth rate itself for different values of β_0 and R.

17.2. Use `baroclinic.m` to see what happens if instead of boundary condition (17.75), the initial value of ψ is kept on the boundaries.

17.3. Explore with `baroclinic.m` the effect of changing the domain width.

17.4. Use `baroclinic.m` and add the beta term to the discretization. Apply the new program to a wide domain and analyze the impact of the beta effect by placing yourself in situations allowing to verify that (17.45) corresponds to the stability limit. If necessary, use the program you constructed for solving Numerical Exercise 17.1.

17.5. Include the possibility of more general interfacial profiles in `baroclinic.m` and analyze a localized baroclinic jet where the interface displacement around mid-depth is

$$a = \frac{f_0 U R}{g'} \tanh\left(\frac{y}{R}\right), \tag{17.78}$$

where R is the internal deformation radius, U the jet velocity, and y the cross-channel coordinate, centered in the middle of the channel.

17.6. Include diagnostics of energy evolution and transfers of energy into `baroclinic.m`. Check to which extent the numerical discretization conserves energy. Verify if another time discretization can improve the simulation.

Joseph Pedlosky
1938–

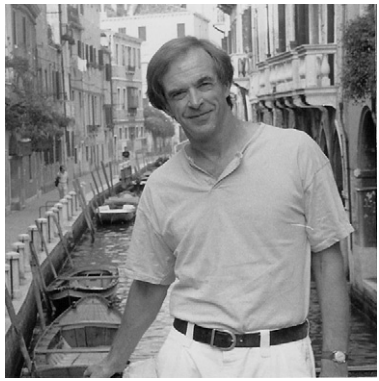

A student of J. G. Charney, Joseph Pedlosky first followed his mentor's footsteps and developed a fascination for baroclinic instability. He quickly became an authority on the subject, having derived new instability criteria and developed a nonlinear theory for growing baroclinic disturbances in nearly inviscid flow. He also made important contributions to the general theory of rotating stratified fluids, the oceanic thermocline, the Gulf Stream, and the general oceanic circulation. In 1979, Pedlosky published the first treatise on Geophysical Fluid Dynamics, which greatly helped codify the discipline.

Pedlosky's approach to research is first to find a problem that is simple enough to be solved completely, yet physically informative, and then to "worry a great deal about it until I could describe the results to an amateur." This incessant quest for clarity has won him great respect as a scientist and much admiration as a speaker. (*Photo credit: J. Pedlosky*)

Peter Broomell Rhines
1942–

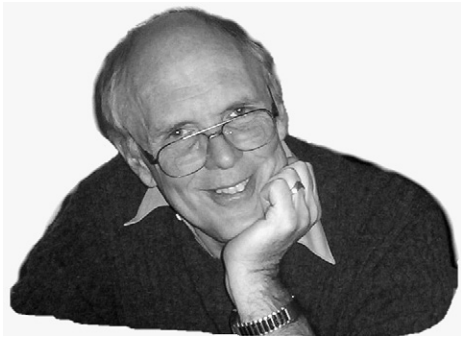

Peter Rhines studied aerospace engineering, but his professors at MIT and Cambridge University exposed him to Rossby waves and potential vorticity, and he became hooked by geophysical fluid dynamics. Over his career, his interests have covered a wide span of geophysical phenomena, ranging from the general ocean circulation and oceanic eddies, to the dynamics of the atmosphere and climate. His approach to questions is equally diverse, replete with paradigm-shifting theories (on potential vorticity homogenization in the ocean), original laboratory experiments, incisive numerical simulations (in geostrophic turbulence), and challenging oceanographic cruises to "white and blue rim of the Arctic world."

The numerous awards Rhines has received emphasize his "amazing physical insight and profound appreciation of observations" and honor his "elegant theoretical studies that have initiated new fields of inquiry." But Rhines remains modest, claiming that "in a sparsely populated discipline like geophysical fluid dynamics, a short life is long enough to work on many aspects of the field." (*Photo courtesy of Peter B. Rhines*)